




Magnetic instability in the spin susceptibility of chiral carbon-based structuresBarbara Montañes ¹, Pábel Machado,¹ Ernesto Medina ^{2,1} and Ismaro Bonalde ^{1,*}¹*Centro de Física, Instituto Venezolano de Investigaciones Científicas, Apartado 20632, Caracas 1020-A, Venezuela*²*Departamento de Física, Colegio de Ciencias e Ingeniería, Universidad San Francisco de Quito, Diego de Robles y Vía Interoceánica, Quito 170901, Ecuador*

(Received 4 March 2024; revised 18 June 2024; accepted 17 July 2024; published 1 August 2024)

Chiral carbon nanostructures have been found to display unexpected magnetic behaviors. Several theoretical calculations performed in the macroscopic limit $\mathbf{q} = 0$ have addressed or predicted some of these findings. To gain more insight into the magnetism of these systems at finite \mathbf{q} , here we use linear response theory to calculate the wave-vector-dependent spin susceptibility $\chi(\mathbf{q}, 0)$ in a half-filling tight-binding model of a helix of carbon atoms with intrinsic spin-orbit coupling (SOC). We find that at the nesting wave number $q = 2k_F$ the paramagnetic state of the system is unstable with respect to the formation of a spin-density-wave type state. Chirality has a small effect on the paramagnetic phase but has no impact on the spin-density-wave type state.

DOI: [10.1103/PhysRevB.110.075101](https://doi.org/10.1103/PhysRevB.110.075101)**I. INTRODUCTION**

Recently, there has been increasing interest in chiral structures with respect to their magnetism and other spin-related properties. Among the systems that have attracted great attention are allotropic modifications of carbon, DNA, polypeptides, and helicenes. Pure carbon allotropes are assumed to be diamagnetic, but magnetic behavior has been observed in many of them. Paramagnetism has been found in helical carbon nanofibers [1,2] and nanosolenoids [3], among others [4], while ferromagnetism has been observed in a variety of all-carbon nanostructures [1,5,6], representing promising nonmetallic magnets for technological applications in spintronic. The origin of ferromagnetism in *sp*-electron carbon materials is unknown, with possible explanations ranging from the presence of impurities to defects to negative curvature. As sample quality has improved, the structural (defects and curvature) argument is favored as the mechanism for this magnetism.

For helical carbon structures, curvature-induced magnetism has been suggested [1,5–9]. Theoretically, a negative curvature in helical structure may be caused by protected carbon radicals and a remote delocalization, which could result in unpaired spins and, therefore, in magnetism. Intrinsic ferromagnetism in helical carbon nanostructures is yet to be confirmed experimentally. So far (to our knowledge) magnetism in pure samples (free of magnetic impurities) has been reported only in Ref. [1]. Most of the time, ferromagnetism

has been attributed to the presence of catalyst's spin particles such as Fe or Ni. Clearly, purer samples need to be examined.

Some kind of magnetism is also found in pure carbon nanotubes, in which chirality is present for the $m \neq n$ closing of the graphene sheet. In these materials, the Fermi energy at $T = 0$ is at the center of the band (half filling). It has been shown theoretically (using band-structure calculations in the macroscopic limit $\mathbf{q} = 0$) and experimentally that for a magnetic field applied along the axis of the nanotube the response is paramagnetic for metallic chiral systems and is diamagnetic for semiconducting chiral ones [9–12]. Interestingly, it was predicted that a small deviation from half filling changes dramatically the longitudinal susceptibility [11].

Other magnetically intriguing helical carbon-based systems are DNA, polypeptides, and helicenes, which show spin-selective property [13] while lacking traditional spin-active interactions such as magnetic centers and strong exchange couplings [14]. The effect, which is still not well understood, is known as chirality-induced spin selectivity (CISS).

The magnetic analyses in the aforementioned systems have been mainly performed in the static $\omega = 0$ and macroscopic limit $\mathbf{q} = 0$ limits, in which the ground states are stable. The scenario for $\mathbf{q} \neq 0$ has been studied mostly in chiral carbon nanotubes and little in the other compounds. We recall the very rich physics that has been found in this region in all kind of low-dimensional systems, with phenomena such as the exciting quantum instabilities charge- and spin-density waves (CDW and SDW) [15,16], Peierls anomaly [17], and Kohn anomaly and Friedel oscillations in the charge density [18].

Most work in the chiral nanotubes has been carried out on the Kohn and Peierls instabilities using density functional theory (DFT) calculations. For an extended review see Ref. [19]. Classic studies on these anomalies in carbon nanotubes with electron-phonon coupling are those of Refs. [20,21]. It is worth mentioning the works on optical phonons of chiral metallic nanotubes at zero and finite temperatures that found a

*Contact author: ijbonalde@gmail.com

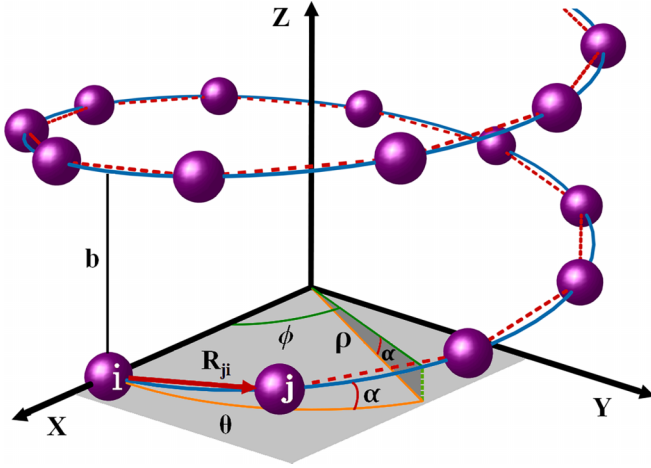


FIG. 1. A helix is described by a pitch b , a radius ρ , and an inclination angle α . All three parameters are defined *positive*. \mathbf{R}_{ji} is a vector joining consecutive carbon sites (i,j); it is the cell parameter.

Kohn anomaly in the LO (axial) branch [22] and on interacting carbon nanotubes with spin-orbit coupling that showed a spin-selective Peierls-type transition [23].

Here, we are interested in the peculiar magnetism of chiral carbon structures at finite \mathbf{q} . To carry out the analysis, we represent these structures by a helix of periodic carbon sites, which is in fact a one-dimensional (1D) system. It is well known that linear chains exhibit magnetic instabilities when $\mathbf{q} \neq 0$, usually as a consequence of electron interactions [15,16,24,25]. In a first approximation, we disregard interactions but include the intrinsic SOC of the system. We calculate the wave-vector-dependent spin susceptibility $\chi(\mathbf{q}, 0)$ of the helix using a half-filling p_z orbital tight-binding Hamiltonian in a linear response theory. This orbital is consistent with the sp^2 hybridization of carbon presents in these materials. That is, we analyze the stability of the paramagnetic state of this 1D chiral metallic system. We perform the calculations in the more natural but seldom used helical coordinate system. We find an antiferromagnetic SDW-type instability at the nesting wave number $q = 2k_F$. Chirality slightly affects the paramagnetic phase but has no impact on the SDW-type state.

II. HELICAL COORDINATE SYSTEM

For convenience, here we adopt the helical coordinate system. Since it is not widely employed, we present a brief description of it. The transformation from helical to cylindrical coordinates is given by [26]

$$\begin{aligned} \rho &= r, \\ \phi &= \theta \text{ (only in magnitude),} \\ \zeta &= z - \frac{b\theta}{2\pi}, \end{aligned} \quad (1)$$

where b is a positive constant defining the helix pitch, as indicated in Fig. 1. Thus, a position vector at any point in helical coordinates is

$$\mathbf{r} = \rho \cos \phi \hat{x} + \rho \sin \phi \hat{y} + \left(\zeta + \frac{b\phi}{2\pi} \right) \hat{z}. \quad (2)$$

From this, we find that the unit vectors for the helical coordinate system are

$$\begin{aligned} \hat{\rho} &= \cos \phi \hat{x} + \sin \phi \hat{y}, \\ \hat{\phi} &= -\cos \alpha \sin \phi \hat{x} + \cos \alpha \cos \phi \hat{y} + \zeta \sin \alpha \hat{z}, \\ \hat{\zeta} &= \hat{z}, \end{aligned} \quad (3)$$

with the scale factors $h_\rho = 1$, $h_\phi = \rho / \cos \alpha$, and $h_\zeta = 1$. The angle α is defined by $\tan \alpha = \frac{b}{2\pi\rho}$, with $0 < \alpha < \pi/2$. We introduce the parameter ζ in the unit vector $\hat{\phi}$ to account for the chirality of the system. In Fig. 1, the helical surfaces are right handed. A positive change in $\hat{\phi}$ with constant $\hat{\zeta}$ implies a positive change in z and $\zeta = 1$ (positive chirality). In left-handed surfaces, a positive change in $\hat{\phi}$ with constant $\hat{\zeta}$ leads to a negative change in z and $\zeta = -1$ (negative chirality). That is, the absence of inversion symmetry in the helix is characterized via the system coordinate $\hat{\phi}$. The unit vectors $\hat{\rho}$, $\hat{\phi}$, and $\hat{\zeta}$ are not all mutually perpendicular ($\hat{\phi} \cdot \hat{\zeta} = \zeta \sin \alpha$), so the helical coordinate system is nonorthogonal. Mathematically, chirality could be described in this nonorthogonal system by the sign of the $x - y$ components of $\hat{\rho} \times \hat{\phi} = \zeta \sin \alpha (\sin \phi \hat{x} - \cos \phi \hat{y}) + \cos \alpha \hat{z}$.

The Pauli matrices in the helical coordinate system are given by

$$\begin{aligned} \sigma_\rho &= \begin{pmatrix} 0 & e^{-i\phi} \\ e^{i\phi} & 0 \end{pmatrix}, \\ \sigma_\phi &= \begin{pmatrix} \zeta \sin \alpha & -i \cos \alpha e^{-i\phi} \\ i \cos \alpha e^{i\phi} & -\zeta \sin \alpha \end{pmatrix}, \\ \sigma_\zeta &= \begin{pmatrix} 1 & 0 \\ 0 & -1 \end{pmatrix}. \end{aligned} \quad (4)$$

Notably, only the component σ_ϕ depends on chirality.

III. MODEL

We follow the tight-binding model for a double helix DNA molecule with one type of nucleotide pair presented in Ref. [27]. This model, developed in cylindrical coordinates, incorporates intrinsic SOC and Rashba-type interactions. Here, we consider a single helix with one type of atom (carbon) and one orbital (p_z) (a one-dimensional periodic chain) and restrict the Hamiltonian to the leading kinetic term and its first correction the intrinsic SOC. We derive the Hamiltonian up to second order in wave vector \mathbf{k} . In our model, neither the kinetic energy nor the intrinsic SOC depends on the chirality ζ , but they are functions of the parameters b and α of the helix (see Appendix).

In line with Ref. [27], we consider a tight-binding Hamiltonian of the form

$$\mathcal{H} = t_i \sum_{\langle ij \rangle} c_i^\dagger c_j + i\lambda_{SO} \sum_{ij} \text{sgn}(j-i) c_i^\dagger \sigma_\phi c_j, \quad (5)$$

where $\langle ij \rangle$ is the nearest neighbor index, c_i^\dagger (c_j) are fermion creation (annihilation) operators at sites \mathbf{r}_i (\mathbf{r}_j), t_i represents the hopping term for π overlaps, λ_{SO} gives the intrinsic spin-orbit strength, and σ_ϕ is one of the Pauli matrices given in (4).

To solve the corresponding Schrödinger equation in \mathbf{k} -space, we assume states that obey Bloch's theorem,

$$\psi_{\mathbf{k}l}(\mathbf{r}) = \frac{1}{\sqrt{N}} \sum_{\mathbf{R}_{ji}} e^{i\mathbf{k}\cdot\mathbf{R}_{ji}} \phi_l(\mathbf{r} - \mathbf{R}_{ji}), \quad (6)$$

where $\phi_l(\mathbf{r} - \mathbf{R}_{ji})$ are the overlapping atomic orbitals, l is the orbital label (in our case $l = p_z$, but we keep the index l for notational ease), and \mathbf{R}_{ji} is the position vector connecting nearest neighbors (see the Appendix). Also, for convenience in performing the calculations, we retain the space vectors in 3D even though our system is 1D. These functions are the basis for the crystal single-particle wave functions (eigenstates)

$$\Psi_{\mathbf{k}}(\mathbf{r}) = a_{\mathbf{k}} \psi_{\mathbf{k}l}(\mathbf{r}), \quad (7)$$

where $a_{\mathbf{k}}$ is the only surviving coefficient of the expansion in our model with one atom and one orbital per atom.

The energy band (eigenvalue) is then calculated as usual by a secular equation (for other carbon systems, see also Refs. [28,29])

$$|\langle \psi_{\mathbf{k}l}(\mathbf{r}) | \mathcal{H} | \psi_{\mathbf{k}l}(\mathbf{r}) \rangle - E(\mathbf{k}) \langle \psi_{\mathbf{k}l}(\mathbf{r}) | \psi_{\mathbf{k}l}(\mathbf{r}) \rangle | a_{\mathbf{k}} = 0. \quad (8)$$

The Hamiltonian matrix elements

$$\begin{aligned} \mathcal{H}_{ll} &= \frac{1}{N} \sum_{\mathbf{R}'_{ji}} \sum_{\mathbf{R}_{ji}} e^{i\mathbf{k}\cdot(\mathbf{R}'_{ji}-\mathbf{R}_{ji})} \\ &\quad \times \langle \phi_l(\mathbf{r} - \mathbf{R}'_{ji}) | \mathcal{H} | \phi_l(\mathbf{r} - \mathbf{R}_{ji}) \rangle \\ &= \sum_{\mathbf{R}_{ji}} e^{i\mathbf{k}\cdot\mathbf{R}_{ji}} \langle \phi_l(\mathbf{r}) | \mathcal{H} | \phi_l(\mathbf{r} - \mathbf{R}_{ji}) \rangle \\ &= \epsilon_{2p}^{\pi} + \sum_{\mathbf{R}_{ji} \neq 0} e^{i\mathbf{k}\cdot\mathbf{R}_{ji}} \langle \phi_l(\mathbf{r}) | \mathcal{H} | \phi_l(\mathbf{r} - \mathbf{R}_{ji}) \rangle, \end{aligned} \quad (9)$$

where ϵ_{2p}^{π} is the on-site energy for orbitals in the same atom and the summation in the second (hopping) term runs only through nearest neighbors. The overlap matrix elements of Eq. (8), in our case of the same orbital on the same atom,

$$\langle \psi_{\mathbf{k}l}(\mathbf{r}) | \psi_{\mathbf{k}l}(\mathbf{r}) \rangle = 1. \quad (10)$$

After calculating the hopping matrix elements, the solution of Eq. (8) yields the eigenvalue in spin space

$$E(\mathbf{k}) = [\epsilon_{2p}^{\pi} + 2t_i f(\mathbf{k})] \mathbf{1}_{\sigma} - 2\lambda_{\text{SO}} g(\mathbf{k}) \sigma_{\phi}, \quad (11)$$

where $f(\mathbf{k}) = \cos(\mathbf{k} \cdot \mathbf{R}_{ji})$ and $g(\mathbf{k}) = \sin(\mathbf{k} \cdot \mathbf{R}_{ji})$ are functions in the reciprocal space. This eigenvalue is similar to the energy found in Ref. [27] without the out-strand and Rashba terms. Then, the diagonalization in spin space leads to the energy spectrum

$$E_s(\mathbf{k}) = \epsilon_{2p}^{\pi} + 2t_i f(\mathbf{k}) - 2s\lambda_{\text{SO}} g(\mathbf{k}), \quad (12)$$

where $s = \pm 1$ represents the spin label. The total wave function is a two-component spinor

$$\Psi_{\mathbf{k}s}(\mathbf{r}) = \frac{\psi_{\mathbf{k}l}(\mathbf{r}) e^{i\frac{\phi}{2}}}{\sqrt{2(1 - s\zeta \sin \alpha)}} \begin{pmatrix} \cos \alpha e^{-i\frac{\phi}{2}} \\ i(s - \zeta \sin \alpha) e^{i\frac{\phi}{2}} \end{pmatrix}. \quad (13)$$

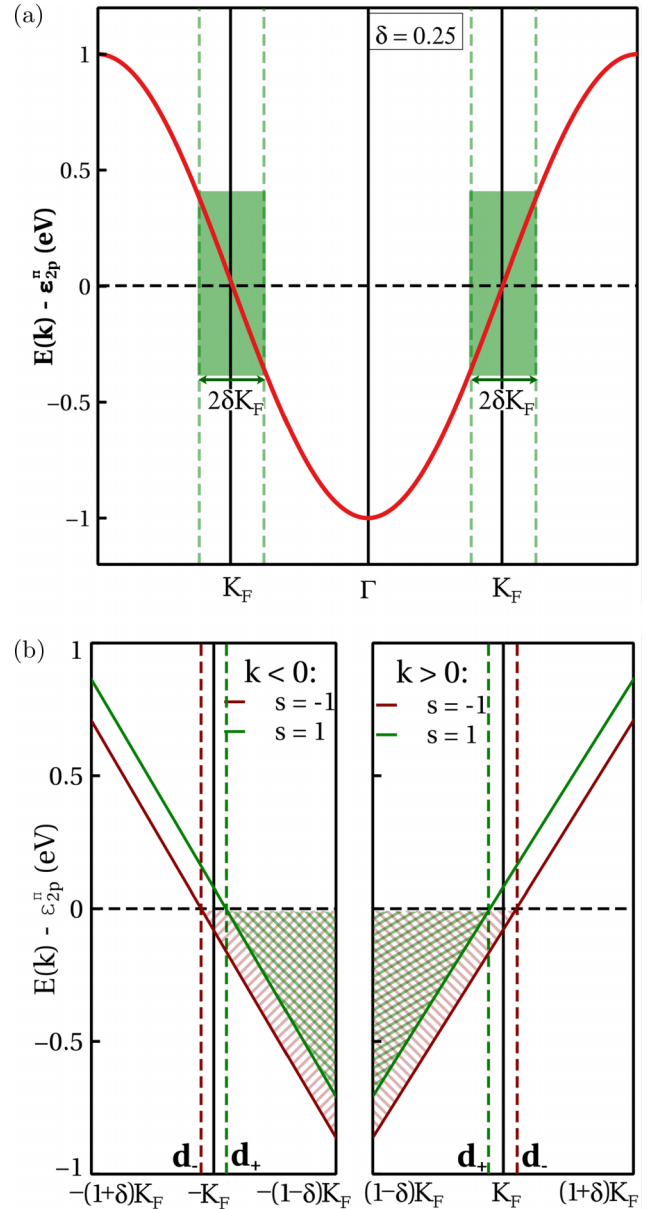


FIG. 2. (a) Kinetic energy band in the first Brillouin zone. The Fermi level, chosen at zero energy, corresponds to $\mathbf{k} = \pm \mathbf{k}_F$. The green areas indicate the region of validity of our tight-binding approximation, where the dispersion relation is linear. (b) The dispersion energy of the helix with spin-orbit coupling in the vicinity of the half-filling point within the region of the linear approximation. Here, $d = 4\lambda_{\text{SO}}/\pi|t_i|$.

In order to perform the calculations in the vicinity of the half-filling point, with the condition $\mathbf{k}_F \cdot \mathbf{R}_{ji} = \nu\pi/2$, we expand $f(\mathbf{k})$ and $g(\mathbf{k})$ around the wave vector \mathbf{k}_F . The parameter $\nu = +1(-1)$ indicates that we carry out the analysis in the positive (negative) wave-vector side of the Brillouin zone, as indicated in Fig. 2(a). We define the wave vector in the vicinity of \mathbf{k}_F as $\mathbf{k}' = \mathbf{k} - \mathbf{k}_F$. Since the system is a helical chain, \mathbf{k} and \mathbf{R}_{ji} lie in the same direction, so $\mathbf{k} \cdot \mathbf{R}_{ji}$ is always positive. In other words, although \mathbf{k} is taken as a three-dimensional vector, only its component parallel to \mathbf{R}_{ji} is relevant and this

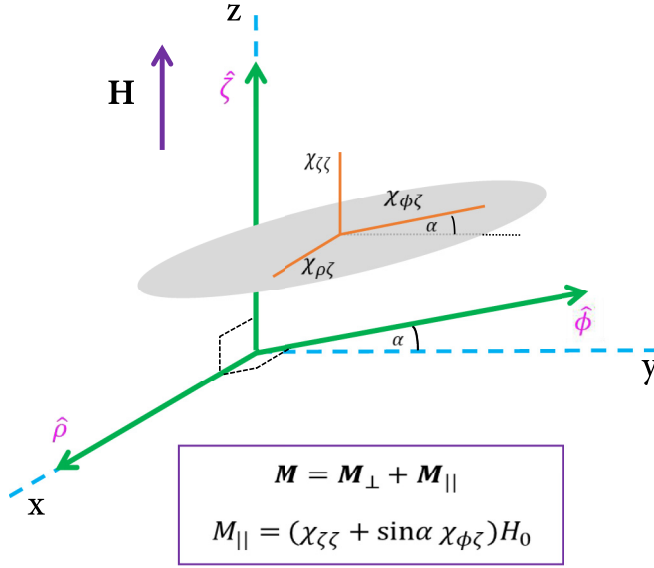


FIG. 3. Magnetization vector in a nonorthogonal helical system with an applied magnetic field along the ζ axis. For the sake of simplicity, the ρ axis is aligned along the x axis of a Cartesian system, so the ϕ axis is in the yz plane. A rotation along the ζ axis does not change M_ζ . H_0 is the field strength.

component is on the axis of symmetry in the 1D Brillouin zone [x axis in Figs. 2(a) and 2(b)]. Then, we expand

$$\begin{aligned} f(\mathbf{k}) &= \cos(\mathbf{k} \cdot \mathbf{R}_{ji}) \approx -\nu \mathbf{k}' \cdot \mathbf{R}_{ji}, \\ g(\mathbf{k}) &= \sin(\mathbf{k} \cdot \mathbf{R}_{ji}) \approx \nu \left(1 - \frac{(\mathbf{k}' \cdot \mathbf{R}_{ji})^2}{2} \right). \end{aligned} \quad (14)$$

These expansions are valid in a region $2\delta k_F$ with $\delta \approx 0.25$, as depicted in Fig. 2(a). In this range, the energy is valid

to order k^2 :

$$E_s(\mathbf{k}') - \epsilon_{2p}^\pi = -2\nu t_i \mathbf{k}' \cdot \mathbf{R}_{ji} - 2s\nu \lambda_{\text{SO}} \left(1 - \frac{(\mathbf{k}' \cdot \mathbf{R}_{ji})^2}{2} \right), \quad (15)$$

where $t_i = -|t_i|$ (see the Appendix). Figure 2(b) depicts the energy dispersion around the half-filling point.

Although the energy spectrum depends on the index ν , it is in fact the same on both sides of the Brillouin zone (Kramers degeneracy, the Hamiltonian (12) is invariant under time reversal). The wave function is the same around each k_F and is not modified by ν . Given the chirality and the choice of the Brillouin side, as usual in the unperturbed system the spin-degeneracy is lifted by the spin-orbit interaction.

IV. LONGITUDINAL SPIN SUSCEPTIBILITY

In our 1D system of carbon atoms with half-filled atomic orbitals we study the stability of the paramagnetic state against the formation of an antiferromagnetic phase. It is necessary to look at the sign of the longitudinal spin susceptibility $\chi_{\parallel}(\mathbf{q}, 0)$ [24,25]. For this purpose, we calculate a general linear response to a small time- and space-dependent external magnetic field $H_0 e^{i(\mathbf{q}' \cdot \mathbf{r} - \omega t)}$ and use the well-known Kubo correlation function in the (\mathbf{q}', ω) domain [30],

$$\begin{aligned} \chi_{\beta\gamma}(\mathbf{q}', \omega) &= i \frac{(g\mu_B)^2}{4\hbar} \int_0^\infty dt e^{i\omega t} \\ &\times \langle \Psi_{p_z k'_s} | [\hat{S}_\beta(\mathbf{q}', t), \hat{S}_\gamma(-\mathbf{q}', 0)] | \Psi_{p_z k'_s} \rangle, \end{aligned} \quad (16)$$

where μ_B is the Bohr magneton, g is the gyromagnetic ratio, $\mathbf{q}' = \mathbf{q} - \mathbf{k}_F$, and the spin density operator

$$\hat{S}_\beta(\mathbf{q}') = \sum_{\mathbf{k}'_s} \sigma_\beta c_{\mathbf{k}'_s}^\dagger c_{\mathbf{k}'_s} \quad (17)$$

with σ_β given in Eq. (4). As for \mathbf{k} , the only relevant component of \mathbf{q} is on the axis of symmetry in the 1D Brillouin zone.

For a magnetic field applied in the ζ direction, the longitudinal magnetization is given by the components $\chi_{\zeta\zeta}$ and $\chi_{\phi\zeta}$ (see Fig. 3). The evaluation of (16) yields the frequency- and wave-vector-dependent longitudinal spin susceptibility

$$\begin{aligned} \chi_{\parallel}(q', \omega) &= -\frac{(g\mu_B)^2}{4} \sum_{\mathbf{k}'} \left[\cos^2 \alpha \left(\frac{n_{\mathbf{k}'+\mathbf{q}'\uparrow} - n_{\mathbf{k}'\downarrow}}{E_{\mathbf{k}'+\mathbf{q}'\uparrow} - E_{\mathbf{k}'\downarrow} + (\hbar\omega - i\eta)} + \frac{n_{\mathbf{k}'+\mathbf{q}'\downarrow} - n_{\mathbf{k}'\uparrow}}{E_{\mathbf{k}'+\mathbf{q}'\downarrow} - E_{\mathbf{k}'\uparrow} + (\hbar\omega - i\eta)} \right) \right. \\ &+ (1 + \zeta) \sin^2 \alpha \left(\frac{n_{\mathbf{k}'+\mathbf{q}'\uparrow} - n_{\mathbf{k}'\uparrow}}{E_{\mathbf{k}'+\mathbf{q}'\uparrow} - E_{\mathbf{k}'\uparrow} + (\hbar\omega - i\eta)} + \frac{n_{\mathbf{k}'+\mathbf{q}'\downarrow} - n_{\mathbf{k}'\downarrow}}{E_{\mathbf{k}'+\mathbf{q}'\downarrow} - E_{\mathbf{k}'\downarrow} + (\hbar\omega - i\eta)} \right) \\ &+ \zeta \sin \alpha \cos \alpha \left(\frac{(1 + \zeta)(n_{\mathbf{k}'+\mathbf{q}'\uparrow} - n_{\mathbf{k}'\uparrow})}{E_{\mathbf{k}'+\mathbf{q}'\uparrow} - E_{\mathbf{k}'\uparrow} + (\hbar\omega - i\eta)} - \frac{(1 + \zeta)(n_{\mathbf{k}'+\mathbf{q}'\downarrow} - n_{\mathbf{k}'\downarrow})}{E_{\mathbf{k}'+\mathbf{q}'\downarrow} - E_{\mathbf{k}'\downarrow} + (\hbar\omega - i\eta)} \right. \\ &\left. \left. + \frac{n_{\mathbf{k}'+\mathbf{q}'\uparrow} + n_{\mathbf{k}'\downarrow}}{E_{\mathbf{k}'+\mathbf{q}'\uparrow} - E_{\mathbf{k}'\downarrow} + (\hbar\omega - i\eta)} - \frac{n_{\mathbf{k}'+\mathbf{q}'\downarrow} + n_{\mathbf{k}'\uparrow}}{E_{\mathbf{k}'+\mathbf{q}'\downarrow} - E_{\mathbf{k}'\uparrow} + (\hbar\omega - i\eta)} \right) \right]. \end{aligned} \quad (18)$$

As opposed to what is obtained in common nonhelical systems, we now have contributions containing sums of probability densities with antiparallel spins [the last two terms in Eq. (18)]. These terms are due to the helical geometry and

not to the nonorthogonality of the reference system (this was checked with orthogonal-helical calculations).

To discuss the magnetic instabilities of a helical chain within the half-filling model at $T = 0$, we analyze the purely

real static limit ($\omega = 0$) of Eq. (18). The Fermi level is defined by the highest energy level of the ground state, which in this case from (15) is $2\lambda_{\text{SO}}$. In the calculation, for example, the integral for $k' < 0$ and spin down goes from $-\delta k_F$ to $-dk_F$

[see Fig. 2(b)] and is restricted by $\frac{q^2}{4k_F^2} > -\frac{2|t_i|}{\pi\lambda_{\text{SO}}} \frac{q'}{k_F} - \frac{8}{\pi^2} + \frac{q^2}{2k_F^2}$. This constraint is satisfied for $|t_i| > \lambda_{\text{SO}}$, which is complied in all known physical systems. Switching to q , an explicit expression for $\chi_{\parallel}(q, 0)$ at $T = 0$ is readily obtained:

$$\begin{aligned} \chi_{\parallel}(q, 0) = & -\frac{(g\mu_B)^2}{8\pi^2\lambda_{\text{SO}}} \left[(\cos\alpha + \zeta \sin\alpha) \left(-\frac{\cos\alpha}{\sqrt{u-v}} \tan^{-1} \left(\frac{(d+\delta)\sqrt{u-v}}{u-v + (\Lambda-d)(\delta+\Lambda)} \right) \right. \right. \\ & + \frac{\cos\alpha}{2\sqrt{u+v}} \ln \left| \frac{(d+\Lambda-\sqrt{u+v})(\delta-\Lambda-\sqrt{u+v})}{(d+\Lambda+\sqrt{u+v})(\delta-\Lambda+\sqrt{u+v})} \right| \\ & + \frac{(1+\zeta)\sin\alpha}{2\Lambda} \ln \left| \frac{\frac{2|t_i|}{\pi\lambda_{\text{SO}}} - \Lambda + d}{\frac{2|t_i|}{\pi\lambda_{\text{SO}}} - \Lambda + \delta} \right| - \frac{(1+\zeta)\sin\alpha}{2\Lambda} \ln \left| \frac{\frac{2|t_i|}{\pi\lambda_{\text{SO}}} + \Lambda + d}{\frac{2|t_i|}{\pi\lambda_{\text{SO}}} + \Lambda - \delta} \right| \Big) \\ & - (\cos\alpha - \zeta \sin\alpha) \left(\frac{\cos\alpha}{2\sqrt{u+v}} \ln \left| \frac{(d+\Lambda+\sqrt{u+v})(\delta+\Lambda-\sqrt{u+v})}{(d+\Lambda-\sqrt{u+v})(\delta+\Lambda+\sqrt{u+v})} \right| \right. \\ & + \frac{\cos\alpha}{\sqrt{u-v}} \tan^{-1} \left(\frac{(-d+\delta)\sqrt{u-v}}{u-v + (\Lambda-d)(\Lambda-\delta)} \right) \\ & \left. \left. - \frac{(1+\zeta)\sin\alpha}{2\Lambda} \ln \left| \frac{\frac{2|t_i|}{\pi\lambda_{\text{SO}}} + \Lambda + d}{\frac{2|t_i|}{\pi\lambda_{\text{SO}}} + \Lambda + \delta} \right| + \frac{(1+\zeta)\sin\alpha}{2\Lambda} \ln \left| \frac{\frac{2|t_i|}{\pi\lambda_{\text{SO}}} - \Lambda + d}{\frac{2|t_i|}{\pi\lambda_{\text{SO}}} - \Lambda + \delta} \right| \right) \right], \end{aligned} \quad (19)$$

where we use the dimensionless parameters

$$\begin{aligned} \Lambda &= \frac{q}{2k_F} - \frac{1}{2} \quad u = \frac{4|t_i|}{\pi\lambda_{\text{SO}}} \left(\frac{q}{2k_F} - \frac{1}{2} \right), \\ v &= \frac{8}{\pi^2} - \left(\frac{q}{2k_F} - \frac{1}{2} \right)^2. \end{aligned} \quad (20)$$

The condition that $\chi_{\parallel}(q, 0)$ is real is satisfied when $u > v$.

V. RESULTS AND DISCUSSION

Equation (19) versus q is plotted in Fig. 4(a) in the vicinity of k_F . Here, we consider that for our model of carbon atoms, with small spin-orbit coupling, the ratio $|t_i|/\lambda_{\text{SO}}$ is large ($|t_i|$ is of the order of eV, while λ_{SO} is in the μeV – meV range [31–33]). We observe in Fig. 4(a) that $\chi_{\parallel}(q, 0)$ is negative for $q/2k_F < 1$, goes through a singularity at $q/2k_F = 1$, and becomes regular and positive for $q/2k_F > 1$. The divergence is present as long as the hopping energy remains much larger than the spin-orbit coupling (that is, for $|t_i| \gg \lambda_{\text{SO}}$), which is a condition always holding for the systems of interest. More importantly, spin-orbit interaction has a negligible effect on the development of the singularity, which can be inferred from $\chi_{\parallel}(q, 0)$ at different values of λ_{SO} and fixed $|t_i| = 1$ eV, as shown in Fig. 4(a). Furthermore, the behavior exhibited in Fig. 4(a) is sustained for vanishing λ_{SO} , limit at which $\chi_{\parallel}(q, 0)$ goes as $1/(\frac{q}{2k_F} - 1)$ in the case $v = 1$.

The present result differs markedly from the logarithmic divergence at $q = 2k_F$ observed in a 1D free-electron gas [see Fig. 4(b)] [30] and in 1D interacting electron systems developing Peierls instabilities [17], CDW and SDW states [15,16], and Kohn anomalies and Friedel oscillations in the charge density [18].

The singularity observed in Fig. 4(a) does imply that the paramagnetic state is unstable against an antiferromagnetic phase around $q = 2k_F$, as indicated by the negative $\chi_{\parallel}(q, 0)$ below this q value [24,25]. As the magnetization $\mathbf{M}(\mathbf{q}) \propto e^{i\mathbf{q}\cdot\mathbf{r}}$, at $q = 2k_F$ for the half-filled band there is a sign change at the neighboring lattice sites and the Fermi surface coincides with the magnetic zone boundary [25]. The divergence separates the negative and positive regions, as expected for deformations that increase energy. The instability is of the SDW type as the Fermi surface satisfies a nesting property, with wave number $Q = 2k_F$ complying with the condition $E_s(k+Q) = -E_s(k)$ for all \mathbf{k} in the energy spectrum (12).

The magnetic instability shown in Fig. 4(a) is similar to those observed and interpreted as SDW behaviors in 3D systems with strong short-range interactions (delta function) [34] and with long-range shielded Coulomb interaction at low densities [24]. Spin-density waves are broken-spin-rotation symmetry ground states of metal which are believed to arise from electron-electron interactions. Thus, the lack of electronic interactions and the negligible contribution of the spin-orbit coupling may cast doubt on the interpretation of the singularity as an evidence of an SDW instability. However, it has been shown that for the special case of one electron per atom, when the band is half full, an SDW instability occurs for vanishing small interaction [25].

The instability of the paramagnetic state at the center of the zone in helical carbon nanostructures is consistent with the prediction of Ref. [11] that a small variation of \mathbf{q} around half filling leads to a substantial change of the longitudinal spin susceptibility. Magnetic behaviors in these systems, both at zero and finite q , may be considered on the basis of the curvature-induced magnetism previously proposed [1,5–9].

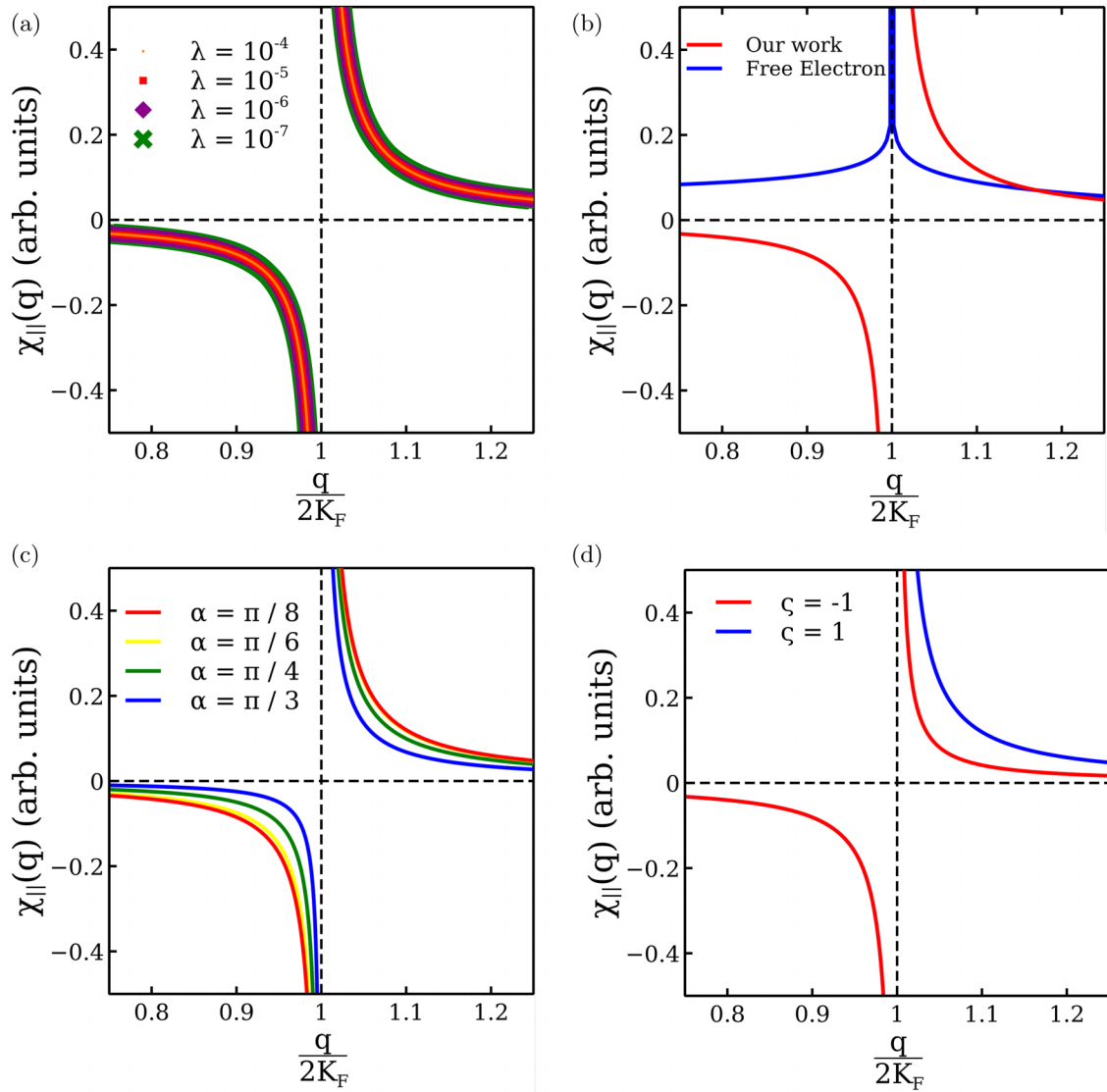


FIG. 4. Longitudinal spin susceptibility of a helical chain at $T = 0$. (a) For three different values of λ_{SO} and $\alpha = 0.25$, $\zeta = 1$, and $|t_i| = 1$ eV. An almost λ_{SO} -independent susceptibility implies that the spin-orbit coupling plays a negligible role in the magnetic properties of a helical carbon-based systems. (b) A helical chain of carbon-like atoms (red curve) as compared to the 1D free-electron model (blue curve). Unlike the helical chain, the free-electron model has a logarithmic divergence at $q = 2k_F$. (c) For different values of α and $\lambda_{\text{SO}} = 0.1$ meV, $\zeta = 1$, and $|t_i| = 1$ eV. A larger effect is observed for $q/2k_F$ as a function of the helix tightening. (d) The effect of chirality (characterized by ζ) on the longitudinal spin susceptibility of a helical chain of carbon-like atoms. No influence is observed for $q/2k_F < 1$ (see text). The curves were obtained for $\alpha = 0.25$, $|t_i| = 1$ eV, and $\lambda_{\text{SO}} = 0.1$ meV.

The singularity found in this work is also similar to that found in 3D nickel at temperatures for which local moments can be established [35]. This case may not be related to our result, because face-centered cubic nickel is completely different from helical carbon nanostructures.

Regarding our result in the context of DNA molecules, a paramagnetic to diamagnetic transition as a function of temperature was found in DNA, which is believed to be a consequence of electron-electron and electron-vibration interactions [36]. This transition is not connected at all with the singularity found here, since electron interactions and finite temperatures are not included. We considered half-filled bands and spin-orbit interactions for a very different scenario.

The helical geometry affects the divergence of the susceptibility of a helical carbon molecule at $q/2k_F$, as shown in

Fig. 4(c). As the helix stretches (larger b), the phases at both sides of $q/2k_F$ seem to be more stable, more so for $q/2k_F < 1$. We note here that extrapolating to $\alpha = 0, \pi/2$ in the final expressions seems a nontrivial limit to take, because a change of symmetry is involved (inversion symmetry is restored and additional degeneracies arise).

Another relevant result is the sensitivity of the magnetic instability to chirality [see Fig. 4(d)]. Chirality shows an effect for wavelength $q > 2k_F$, but no impact for $q < 2k_F$. This is surprising, although it could simply be another manifestation of the formation of the SDW state. The paramagnetic state responds more readily to an external field (is less stable) when the helical carbon chain is oriented clockwise (positive chirality) than when it is oriented counterclockwise (negative chirality). On the other hand, once the antiferromagnetic SDW

state becomes favorable upon application of a magnetic field with modulation $q < 2k_F$, the magnetic response is independent of the helical chain orientation. This could be due to the fact that an SDW state is represented by two density waves for spin up and spin down with modulation of wavelength $2k_F$ and a phase shift. In the SDW phase the two density waves with opposite spins can balance their contributions under a chirality change and thus the system response becomes independent of it.

Finally, it is worth mentioning that the divergence has mirror-plane symmetry with respect to the Γ point of the Brillouin zone, as expected given the periodicity of the system.

VI. CONCLUSIONS

We used a linear response approach to calculate at $T = 0$, in a helical coordinate system and near the half-filled band, the magnetic response to a wave-vector-dependent external field of a helical carbon-based structure. It was assumed that carbon atoms have intrachain coupling with electrons shared by atoms in the π cloud contributing to atomic spin-orbit coupling. The calculations yield a spin susceptibility that diverges at $q = 2k_F$, pointing to an instability of the paramagnetic state and the formation of an SDW-type state. Chirality slightly affects the response in the paramagnetic phase, but does not influence the antiferromagnetic SDW-type state. Intrinsic spin-orbit coupling has negligible effects on spin susceptibility.

ACKNOWLEDGMENT

E.M. acknowledges support from POLIGRANT 17617 from USFQ.

APPENDIX: TIGHT-BINDING AND SPIN-ORBIT PARAMETERS IN THE HELICAL COORDINATE SYSTEM

We show here that the physics of the tight-binding and spin-orbit constants are naturally derived in the helical coordinate system. For this, we start with the overlap between orbitals at i and j sites [27],

$$\mathbf{E}_{\mu,\mu'}^{i,j} = (\hat{\mathbf{n}}(\mu_i), \hat{\mathbf{n}}(\mu_j))V_{\mu\mu'}^\pi + \frac{(\mathbf{R}_{ji}, \hat{\mathbf{n}}(\mu_i))(\mathbf{R}_{ji}, \hat{\mathbf{n}}(\mu_j))}{(\mathbf{R}_{ji}, \mathbf{R}_{ji})}(V_{\mu\mu'}^\sigma - V_{\mu\mu'}^\pi), \quad (\text{A1})$$

and consider all vectors here in helical coordinates. The unit vectors $\hat{\mathbf{n}}(\mu_j)$ in the direction of the orbital μ_j

$$\begin{aligned} \hat{\mathbf{n}}(p_x, i) &= \cos \phi_i \hat{x} + \sin \phi_i \hat{y}, \\ \hat{\mathbf{n}}(p_y, i) &= \cos(\alpha)(-\sin \phi_i \hat{x} + \cos \phi_i \hat{y}) + \zeta \sin \alpha \hat{z}, \\ \hat{\mathbf{n}}(p_z, i) &= \hat{z}. \end{aligned} \quad (\text{A2})$$

From Eq. (2) we have that the position vector connecting nearest neighbors \mathbf{R}_{ij} is given by

$$\begin{aligned} \mathbf{R}_{ji} &= -2\rho \sin^2 \left(\frac{\Delta\phi}{2} \right) \hat{\rho} \\ &+ \left(\rho \sin(\Delta\phi) \cos \alpha + \frac{\zeta b \Delta\phi}{2\pi} \sin \alpha \right) \hat{\phi} + \frac{b \Delta\phi}{2\pi} \hat{\zeta}, \end{aligned} \quad (\text{A3})$$

where $\Delta\phi = \theta_j - \theta_i$ is the angle between the neighbors at sites i and j (see Fig. 1). Therefore, its magnitude is

$$|\mathbf{R}_{ji}| = \rho \sqrt{2(1 - \cos \Delta\phi) + (\Delta\phi \tan \alpha)^2}. \quad (\text{A4})$$

The overlap components are then

$$\mathbf{E}_{x,x}^{i,j} = \frac{\cos(\Delta\phi)|\mathbf{R}_{ji}|^2 V_{pp}^\pi - 4\rho^2 \sin^4 \left(\frac{\Delta\phi}{2} \right) (V_{pp}^\sigma - V_{pp}^\pi)}{|\mathbf{R}_{ji}|^2}, \quad (\text{A5})$$

$$\begin{aligned} \mathbf{E}_{y,y}^{i,j} &= (\cos^2 \alpha \cos(\Delta\phi) + \sin^2 \alpha) V_{pp}^\pi \\ &- \frac{(\rho \cos \alpha \sin(\Delta\phi) + \zeta \frac{b \Delta\phi}{2\pi} \sin \alpha) (V_{pp}^\sigma - V_{pp}^\pi)}{|\mathbf{R}_{ji}|^2}, \end{aligned} \quad (\text{A6})$$

$$\mathbf{E}_{z,z}^{i,j} = V_{pp}^\pi - \frac{(b \Delta\phi)^2 (V_{pp}^\sigma - V_{pp}^\pi)}{4\pi^2 |\mathbf{R}_{ij}|^2}, \quad (\text{A7})$$

$$\begin{aligned} \mathbf{E}_{x,y}^{i,j} &= \cos \alpha \sin \Delta\phi V_{pp}^\pi \\ &- \frac{2\rho^2 \sec \alpha \sin \Delta\phi \cos^2 \alpha \sin^2 \left(\frac{\Delta\phi}{2} \right) (V_{pp}^\sigma - V_{pp}^\pi)}{|\mathbf{R}_{ji}|^2} \\ &- \frac{2\rho^2 \sec \alpha \Delta\phi \sin^2 \alpha \sin^2 \left(\frac{\Delta\phi}{2} \right) (V_{pp}^\sigma - V_{pp}^\pi)}{|\mathbf{R}_{ji}|^2}, \end{aligned} \quad (\text{A8})$$

$$\mathbf{E}_{x,z}^{i,j} = -\frac{2\rho^2 \Delta\phi \tan \alpha \sin^2 \left(\frac{\Delta\phi}{2} \right) (V_{pp}^\sigma - V_{pp}^\pi)}{|\mathbf{R}_{ji}|^2}, \quad (\text{A9})$$

$$\begin{aligned} \mathbf{E}_{y,z}^{i,j} &= \zeta \sin(\alpha) V_{pp}^\pi + \frac{\rho b \Delta\phi \sec \alpha \sin \Delta\phi \cos^2 \alpha (V_{pp}^\sigma - V_{pp}^\pi)}{2\pi |\mathbf{R}_{ji}|^2} \\ &+ \frac{\rho b \Delta\phi \sec \alpha \zeta \Delta\phi \sin^2 \alpha (V_{pp}^\sigma - V_{pp}^\pi)}{2\pi |\mathbf{R}_{ji}|^2}. \end{aligned} \quad (\text{A10})$$

From the component $\mathbf{E}_{z,z}^{i,j}$ (A7) we find the hopping constant

$$t_i = V_{pp}^\pi - \frac{(\Delta\phi \tan \alpha)^2 (V_{pp}^\sigma - V_{pp}^\pi)}{2(1 - \cos \Delta\phi) + (\Delta\phi \tan \alpha)^2}, \quad (\text{A11})$$

and from the component $\mathbf{E}_{y,z}^{i,j}$ (A10) the helical spin-orbit coupling

$$\lambda_{\text{SO}} = \frac{\xi_p \Delta\phi \tan \alpha (1 - \cos \Delta\phi) (V_{pp}^\sigma - V_{pp}^\pi)}{(\epsilon_{2p}^\pi - \epsilon_{2p}^\sigma) [2(1 - \cos \Delta\phi) + (\Delta\phi \tan \alpha)^2]}. \quad (\text{A12})$$

Usually, $|V_{pp}^\sigma| > |V_{pp}^\pi|$ and $V_{pp}^\pi < 1$ [29], then $t_i < 0$ and $\lambda_{\text{SO}} > 0$. We see that even though both the hopping constant and the spin-orbit coupling depend on the helix structure (through α), they are not influenced by chirality. If $\alpha = 0$, no helix (the system is just a stack of rings), the hopping constant t_i becomes equal to the Slater-Koster π overlap V_{pp}^π and the intrinsic λ_{SO} goes to zero.

- [1] Y. Zhuang, J. Wen, N. Tang, M. Li, L. Lv, and Y. Du, *AIP Adv.* **3**, 052112 (2013).
- [2] X. Li and Z. Xu, *Mater. Res. Bull.* **47**, 4383 (2012).
- [3] J. Wang, Y. Zhu, G. Zhuang, Y. Wu, S. Wang, P. Huang, G. Sheng, M. Chen, S. Yang, T. Greber, and P. Du, *Nat. Commun.* **13**, 1239 (2022).
- [4] T. L. Makarova, *Semiconductors* **38**, 615 (2004).
- [5] R. Caudillo, X. Gao, R. Escudero, M. José-Yacamán, and J. B. Goodenough, *Phys. Rev. B* **74**, 214418 (2006).
- [6] N. Park, M. Yoon, S. Berber, J. Ihm, E. Osawa, and D. Tomanek, *Phys. Rev. Lett.* **91**, 237204 (2003).
- [7] Y. Kopelevich, R. R. da Silva, J. H. S. Torres, A. Penicaud, and T. Kyotani, *Phys. Rev. B* **68**, 092408 (2003).
- [8] S. Ihara, S. Itoh, and J. I. Kitakami, *Phys. Rev. B* **48**, 5643 (1993).
- [9] C. C. Tsai, S. C. Chen, F. L. Shyu, C. P. Chang, and M. F. Lin, *Phys. E* **30**, 86 (2005).
- [10] T. A. Searles, Y. Imanaka, T. Takamasu, H. Ajiki, J. A. Fagan, E. K. Hobbie, and J. Kono, *Phys. Rev. Lett.* **105**, 017403 (2010).
- [11] J. P. Lu, *Phys. Rev. Lett.* **74**, 1123 (1995).
- [12] H. Ajiki and T. Ando, *J. Phys. Soc. Jpn.* **64**, 4382 (1995).
- [13] R. Naaman and D. H. Waldeck, *Annu. Rev. Phys. Chem.* **66**, 263 (2015).
- [14] F. Evers *et al.*, *Adv. Mater.* **34**, 2106629 (2022).
- [15] A. W. Overhauser, *Phys. Rev. Lett.* **4**, 462 (1960).
- [16] A. W. Overhauser, *Phys. Rev.* **128**, 1437 (1962).
- [17] R. E. Peierls, *Quantum Theory of Solids* (Clarendon, Oxford, 1955).
- [18] W. A. Harrison, *Solid State Theory* (Dover, New York, 1979).
- [19] J.-C. Charlier, X. Blase, and S. Roche, *Rev. Mod. Phys.* **79**, 677 (2007).
- [20] J. W. Mintmire, B. I. Dunlap, and C. T. White, *Phys. Rev. Lett.* **68**, 631 (1992).
- [21] R. Saito, M. Fujita, G. Dresselhaus, and M. S. Dresselhaus, *Phys. Rev. B* **46**, 1804 (1992).
- [22] S. Piscanec, M. Lazzeri, J. Robertson, A. C. Ferrari, and F. Mauri, *Phys. Rev. B* **75**, 035427 (2007).
- [23] B. Braunecker, G. I. Japaridze, J. Klinovaja, and D. Loss, *Phys. Rev. B* **82**, 045127 (2010).
- [24] D. R. Hamann and A. W. Overhauser, *Phys. Rev.* **143**, 183 (1966).
- [25] D. R. Penn, *Phys. Rev.* **142**, 350 (1966).
- [26] R. A. Waldron, *Q. J. Mech. Appl. Math.* **11**, 438 (1958).
- [27] S. Varela, V. Mujica, and E. Medina, *Phys. Rev. B* **93**, 155436 (2016).
- [28] E. McCann, Electronic properties of monolayer and bilayer graphene, in *Graphene Nanoelectronics*, edited by H. Raza (Springer-Verlag, Berlin, 2012), Chap. 8, p. 237.
- [29] R. Saito, M. S. Dresselhaus, and G. Dresselhaus, *Physical Properties of Carbon Nanotubes* (Imperial College Press, London, 1998).
- [30] G. F. Giuliani and G. Vignale, *Quantum Theory of the Electron Liquid* (Cambridge University Press, Cambridge, 2005).
- [31] M. Gmitra, S. Konschuh, C. Ertler, C. Ambrosch-Draxl, and J. Fabian, *Phys. Rev. B* **80**, 235431 (2009).
- [32] W. Izumida, K. Sato, and R. Saito, *J. Phys. Soc. Jpn.* **78**, 074707 (2009).
- [33] G. A. Steele, F. Pei, E. A. Laird, J. M. Jol, H. B. Meerwaldt, and L. P. Kouwenhoven, *Nat. Commun.* **4**, 1573 (2013).
- [34] D. R. Hamann, Ph.D. thesis, Massachusetts Institute of Technology, 1966.
- [35] J. Staunton, B. L. Gyorffy, G. M. Stocks, and J. Wadsworth, *J. Phys. F: Met. Phys.* **16**, 1761 (1986).
- [36] V. Apalkov and T. Chakraborty, *Phys. Rev. B* **78**, 104424 (2008).